10210-68-1; $[(triphos)Co(O_2C_7H_5)]^{2+}$, 110315-85-0; $[(triphos)Co(O_2C_7H_5)]$, 110315-86-1; $[(triphos)Co(3,5\text{-}DBQ)]^{3+}$, 110315-96-3; $[(triphos)Co(3,5\text{-}DBSQ)]^{2+}$, 110315-98-5; $[(triphos)Co(3,5\text{-}DBCat)]$, 110352-17-5; $[(triphos)Co(3,5\text{-}DBCat)]^-$, 110315-87-2; $[(triphos)Co(o\text{-}Cl_4Q)]^{3+}$, 110315-95-2; $[(triphos)Co(o\text{-}Cl_4SQ)]^{2+}$, 110315-97-4; $[(triphos)Co(o\text{-}Cl_4Cat)]$, 110453-57-1; $[(triphos)Co(o\text{-}Cl_4Cat)]^-$, 110315-88-3; $[(triphos)Co(phenQ)]^{3+}$, 110315-99-6; $[(triphos)Co(phenSQ)]^{2+}$, 110316-00-2; $[(triphos)Co(phenCat)]$, 110432-95-6; $[(triphos)Co(phenCat)]^-$, 110315-89-4; $[H_3Co(Cat)]^{3+}$, 110315-90-7; $[H_3Co(Cat)]^{2+}$, 110315-91-8; $[H_3Co(Cat)]^+$, 110315-92-9; $[H_3Co(Cat)]$, 110315-93-0; $[H_3Co(Cat)]^-$, 110315-94-1.

Supplementary Material Available: Listings of hydrogen atom coordinates and final anisotropic and isotropic thermal parameters for **2** (6 pages); a listing of observed and calculated structure factors (30 pages). Ordering information is given on any current masthead page.

Contribution from the Department of Chemistry, Harvard University, Cambridge, Massachusetts 02138, and Molecular Structure Center, Indiana University, Bloomington, Indiana 47405

Synthesis and Structural Characterization of $[Re_2(\mu\text{-}O)_2O_2(CH_2CMe_3)_4]$ and the Li^+ and $[NEt_4]^+$ Salts of the d^2 $[ReO_2(CH_2CMe_3)_2]^-$ Anion

Shiang Cai,† David M. Hoffman,*† John C. Huffman,‡ Derk A. Wierda,† and Hee-Gweon Woo†

Received November 26, 1986

At room temperature, $[Re(OSiMe_3)O_3]$ reacts with 1.5 equiv of $Al(CH_2CMe_3)_3(THF)$ in hexane to give d^1–d^1 $[Re_2(\mu\text{-}O)_2O_2(CH_2CMe_3)_4]$ in 43% yield. $[Re_2(\mu\text{-}O)_2O_2(CH_2CMe_3)_4]$ adopts a structure in which two square-pyramidal Re centers are linked via bridging oxo ligands. At each Re center, the two bridging oxo ligands and two terminal alkyl ligands define the square plane and another oxo ligand occupies the apical position. The Re–Re distance of 2.606 (2) Å is consistent with a Re–Re single bond. The complex $[Re_2(\mu\text{-}O)_2O_2(CH_2CMe_3)_4]$ is reduced with Li/Hg or Na/Hg to give diamagnetic $M[ReO_2(CH_2CMe_3)_2]$ in 66% (M = Li) and 75% (M = Na) yield. The $[NEt_4]^+$ salt is prepared by cation exchange involving the Na^+ salt. An X-ray structure determination of the lithium salt shows that in the solid state the complex is properly formulated as $\{[Li(CH_3CN)_2][ReO_2(CH_2CMe_3)_2]\}_2$. The structure consists of two $[ReO_2(CH_2CMe_3)_2]^-$ anions linked by two bridging $[Li(CH_3CN)_2]^+$ cations bonded to the oxo ligands. The anions are distorted from a tetrahedral geometry with C–Re–C and O–Re–O angles of 83.7 (5) and 134.9 (4)°, respectively. The structure determination of the tetraethylammonium salt also revealed a distorted $[ReO_2(CH_2CMe_3)_2]^-$ anion with C–Re–C and O–Re–O angles of 81.2 (5) and 127.5 (4)°, respectively. Calculations of the extended Hückel type show that the geometry of $[ReO_2H_2]^-$, a model for $[ReO_2(CH_2CMe_3)_2]^-$, is controlled by the HOMO. The HOMO is stabilized by a reduction in π antibonding between the Re and oxo ligands when the complex is distorted from a tetrahedral geometry. Crystal data for $[Re_2(\mu\text{-}O)_2O_2(CH_2CMe_3)_4]$ at −155 °C: a = 20.491 (9) Å, b = 20.705 (9) Å, c = 5.935 (2) Å, Z = 4, d_{calcd} = 1.902 g cm^{-3}, and space group $P2_1nb$. Crystal data for $\{[Li(CH_3CN)_2][ReO_2(CH_2CMe_3)_2]\}_2$ at −155 °C: a = 12.309 (3) Å, b = 16.662 (4) Å, c = 9.842 (2) Å, β = 108.58 (1)°, Z = 4, d_{calcd} = 1.561 g cm^{-3}, and space group $P2_1/a$. Crystal data for $[NEt_4][ReO_2(CH_2CMe_3)_2]$ at −145 °C: a = 9.962 (7) Å, b = 21.276 (15) Å, c = 10.552 (8) Å, β = 96.44 (3)°, Z = 4, d_{calcd} = 1.467 g cm^{-3}, and space group $P2_1/n$.

Introduction

As a part of a general study of the chemistry of transition-metal oxo–alkyl complexes, we have been examining the metal–oxygen and metal–ligand/substrate bond reactivity in rhenium oxo–alkyl compounds. Our choice of this specific class of compounds was based upon the extensive reactivity of the Re–O bonds observed in the $[(\eta^5\text{-}C_5Me_5)ReO_x]$ systems[1] and the available reactive Re–C bond. During the course of our studies, we decided to prepare oxo–alkyl anion complexes with the expectation that they would be reactive toward electrophiles at the oxo ligand site and could be used as precursors for the synthesis of heterobimetallic oxo complexes.[2] In this paper we describe the synthesis of the new d^2 four-coordinate complex $[ReO_2(CH_2CMe_3)_2]^-$ by reduction of the Re(VI) complex $[Re_2(\mu\text{-}O)_2O_2(CH_2CMe_3)_4]$. We also report the structure of $[Re_2(\mu\text{-}O)_2O_2(CH_2CMe_3)_4]$ and the structures of the lithium and tetraethylammonium salts of $[ReO_2(CH_2CMe_3)_2]^-$.

There are relatively few other second- and third-row d^2 four-coordinate transition-metal complexes that have been structurally characterized, and all of the compounds are homoleptic with π-donor ligands. The geometries range from elongated tetrahedral to flattened tetrahedral.[3] In all of the complexes there is significant metal–ligand π bonding since the compounds are diamagnetic, and it is clear that π bonding is an important driving force in setting the geometries. The results of our crystallographic studies coupled with molecular orbital calculations show that the structure of $[ReO_2(CH_2CMe_3)_2]^-$ is also strongly influenced by the π-donating oxo ligands.

Experimental Section

General Techniques. All operations were performed under an atmosphere of dry N_2 or Ar or under vacuum. Solvents were dried and degassed in the usual manner. ^1H and ^{13}C NMR spectra were recorded on Bruker 250- or 300-MHz spectrometers. The ^1H NMR chemical shifts are reported relative to the ^1H impurities in the solvents (toluene-d_8, δ 2.09; CD_3CN, δ 1.93), and ^{13}C NMR chemical shifts are reported relative to the methyl carbon septets of toluene-d_8 set at δ 20.40 and of CD_3CN set at δ 1.30. Infrared spectra were recorded on a Perkin-Elmer 683 spectrometer and are referenced externally to the 1601-cm^{-1} band of polystyrene. Microanalyses were performed by Dornis and Kolbe, Mulheim a. d. Ruhr 1, Federal Republic of Germany, Galbraith Microanalytical Laboratory, Knoxville, TN, and Multichem Laboratory, Lowell, MA.

Electrochemical studies were performed with a Princeton Applied Research Model 370 electrochemistry system. A Beckman platinum electrode was used as the working electrode with a platinum wire as the counter electrode. Potentials are referenced versus the standard calomel electrode. Experiments were performed on 10^{-3} M solutions of compound with 0.1 M $[N\text{-}n\text{-}Bu_4][ClO_4]$ as supporting electrolyte.

$[Re_2(\mu\text{-}O)_2O_2(CH_2CMe_3)_4]$. Method A. In a Schlenk flask, $[ReO_3(OSiMe_3)]$ (1.59 g, 4.92 mmol) was dissolved in 60 mL of hexane and

† Harvard University.
‡ Indiana University.

(1) A review article has been published: Herrmann, W. A. *J. Organomet. Chem.* **1986**, *300*, 111.
(2) Two anionic oxo–alkyl complexes of rhenium have recently been structurally characterized: Stavropoulos, P.; Edwards, P. G.; Wilkinson, G.; Motevalli, M.; Malik, K. M. A.; Hursthouse, M. B. *J. Chem. Soc., Dalton Trans.* **1985**, 2167.
(3) (a) Otsuka, S.; Kamata, M.; Hirotsu, K.; Higuchi, T. *J. Am. Chem. Soc.* **1981**, *103*, 3011. (b) Chisholm, M. H.; Cotton, F. A.; Extine, M. W. *Inorg. Chem.* **1978**, *17*, 1329. Bradley, D. C.; Chisholm, M. H. *J. Chem. Soc. A* **1971**, 2741. (c) Roland, E.; Walborsky, E. C.; Dewan, J. C.; Schrock, R. R. *J. Am. Chem. Soc.* **1985**, *107*, 5795. (d) Listemann, M. L.; Dewan, J. C.; Schrock, R. R. *J. Am. Chem. Soc.* **1985**, *107*, 7207.

0020-1669/87/1326-3693$01.50/0

Table I. Crystal Data Summary for $[Re_2(\mu\text{-}O)_2O_2(CH_2CMe_3)_4]$ (**1**), $\{[Li(CH_3CN)_2][ReO_2(CH_2CMe_3)_2]\}_2$ (**2a**), and $[NEt_4][ReO_2(CH_2CMe_3)_2]$ (**2c**)

	1	2a	2c
color of cryst	yellow	green	green
cryst dimens, mm	0.07 × 0.07 × 0.09	0.12 × 0.12 × 0.15	0.07 × 0.06 × 0.13
space group	$P2_1nb$	$P2_1/a$	$P2_1/n$
cell dimens			
temp, °C	−155	−155	−145
a, Å	20.491 (9)	12.309 (3)	9.962 (7)
b, Å	20.705 (9)	16.662 (4)	21.276 (15)
c, Å	5.935 (2)	9.842 (2)	10.552 (8)
β, deg		108.58 (1)	96.44 (3)
Z (molecules/cell)	4	4	4
vol, Å^3	2518.15	1913.31	2222.33
D_{calcd}, g cm^{-3}	1.902	1.561	1.467
wavelength, Å	0.710 69	0.710 69	0.710 69
linear abs coeff, cm^{-1}	97.568	64.384	55.504
detector to sample dist, cm	22.5	22.5	22.5
sample to source dist, cm	23.5	23.5	23.5
takeoff angle, deg	2.0	2.0	2.0
average ω-scan width at half-height, deg	0.25	0.25	0.25
scan speed, deg min^{-1}	4.0	4.0	4.0
scan width, deg (+dispersion)	2.0	2.0	2.0
single bkgd time at extremes of scan, s	6	8	6
aperture size, mm	3.0 × 4.0	3.0 × 4.0	3.0 × 4.0
2*θ* range, deg	6–45	6–45	6–45
total no. of rflns collected	2863	2814	3260
no. of unique rflns	1710	2501	2913
no. with $F_0 > 3.00\sigma(F_0)$	1605	2027	2410
$R(F)$	0.0466	0.0463	0.0440
$R_w(F)$	0.0443	0.0442	0.0419
goodness of fit for last cycle	1.280	1.045	1.003
largest Δ/s for last cycle	0.05	0.05	0.05

cooled to −20 °C.[4] To the cold solution was slowly added a solution of $Al(CH_2CMe_3)_3(THF)$ (2.32 g, 7.42 mmol) in 25 mL of hexane to give a red-orange solution. After the addition was complete, the solution was stirred at room temperature under N_2 for 12 h. The mixture was then chromatographed on Al_2O_3 (activity grade V; hexane eluant) under N_2. A single yellow band was observed and collected. The hexane solution volume was reduced under vacuum and then cooled to −80 °C. This yielded yellow needles that were isolated by removing the supernatant liquid via cannula and dried under vacuum; yield 0.77 g, 43%.

Method B. An analogous procedure employing $Zn(CH_2CMe_3)_2$ gave an isolated yield of 25%. Anal. Calcd for $C_{20}H_{44}O_4Re_2$: C, 33.32; H, 6.15. Found: C, 33.87; H, 6.13. ^{1}H NMR (C_7D_8): δ 3.63 and 3.10 (d of an AB q, 8, J_{HH} = 12 Hz, CH_2CMe_3), 1.42 (s, 36, CH_2CMe_3). ^{13}C NMR (C_7D_8): δ 70.86 (t, J_{CH} = 128.5 Hz, CH_2CMe_3), 37.58 (s, CH_2CMe_3), 33.46 (q, J_{CH} = 125.2 Hz, CH_2CMe_3). IR (KBr pellet, cm^{-1}): ν(Re=O) = 1027 s and 1013 s (ν(Re=^{18}O) = 966 and 957); ν(Re—O) = 755 m (ν(Re—^{18}O) = 708); ν(Re—O) = 514 w (ν(Re—^{18}O) = 496); 1477 s, 1469 s, 1464 s, 1447 m, 1394 s, 1369 s, 1271 w, 1239 s, 1224 sh, 1166 m, 1151 m, 1110 w, 939 w, 910 w, 636 m, 395 w.

$[Re_2(\mu\text{-}^{18}O)_2{}^{18}O_2(CH_2CMe_3)_4]$. This complex was prepared by stirring $[Re_2(\mu\text{-}O)_2O_2(CH_2CMe_3)_4]$ with 100 equiv of $^{18}OH_2$ in THF for 18 h.

$Li[ReO_2(CH_2CMe_3)_2]$. To a yellow solution of $[Re_2(\mu\text{-}O)_2O_2(CH_2CMe_3)_4]$ (0.123 g, 0.17 mmol) in pentane (20 mL) was added Li/Hg (0.014%, 0.007 g, 1.01 mmol). A green solid immediately deposited. The reaction mixture was further stirred until the supernatant liquid was colorless. The solvent was then removed under vacuum and the residue extracted with CH_3CN (1 × 20 mL, 2 × 5 mL) and filtered. The clear green filtrate was reduced in volume to 5 mL under vacuum and then cooled to −20 °C. This produced green crystals that were isolated by removing the supernatant via cannula and dried under vacuum. An X-ray crystallography study showed that there are two acetonitrile molecules per anion present in the crystals. Under vacuum the crystals powdered as the solvent was removed from the lattice. An analysis of the IR spectrum indicated that no acetonitrile was present for solids held under vacuum for >12 h, but a satisfactory analysis was not obtained (four attempts on four different batches); yield 0.083 g, 66%. ^{1}H NMR (CD_3CN): δ 3.62 (s, 4, CH_2CMe_3), 0.97 (s, 18, CH_2CMe_3). ^{13}C{^{1}H} NMR (CD_3CN): δ 39.18 (s, CH_2CMe_3), 33.71 (s, CH_2CMe_3), 33.55 (s, CH_2CMe_3). IR (Nujol, KBr, cm^{-1}): ν(Re=O) = 948 s and 851 s; 1362 m, 1306 w, 1240 m, 1149 w, 1131 w, 1019 m, 1003 w, 666 w, 546 w.

$Na[ReO_2(CH_2CMe_3)_2]$. A procedure similar to the one used for the synthesis of the Li salt was followed. In a typical reaction, $[Re_2(\mu\text{-}O)_2O_2(CH_2CMe_3)_4]$ (0.157 g, 0.22 mmol) was stirred with Na/Hg (0.020%, 0.010 g, 0.43 mmol) in pentane. Workup and crystallization from a mixture of CH_3CN and toluene produced green needles. NMR analysis for inert-gas-dried crystals showed that approximately two acetonitrile molecules per anion are present in the crystals. The crystals powdered under vacuum as the acetonitrile was removed from the lattice. Analytical and IR analyses for samples held under vacuum for >12 h showed that the acetonitrile was completely removed; yield 0.126 g, 75%. Anal. Calcd for $C_{10}H_{22}NaO_2Re$: C, 31.37; H, 5.78; N, 0.00. Found: C, 31.27; H, 5.74; N, 0.00. ^{1}H NMR (CD_3CN): δ 3.30 (s, 4, CH_2CMe_3), 0.94 (s, 18, CH_2CMe_3). ^{13}C{^{1}H} NMR (CD_3CN): δ 38.18 (s, CH_2CMe_3), 34.95 (s, CH_2CMe_3), 33.84 (s, CH_2CMe_3). IR (Nujol, KBr, cm^{-1}): ν(Re=O) = 946 s and 854 s; 1358 m, 1304 w, 1240 m, 1153 w, 1136 w, 985 w.

$[NEt_4][ReO_2(CH_2CMe_3)_2]$. In a 50-mL Schlenk flask was placed $Na[ReO_2(CH_2CMe_3)_2]$ (0.060 g, 0.16 mmol) and $[NEt_4]Br$ (0.033 g, 0.16 mmol). The mixture was dissolved in CH_3CN (20 mL) and then stirred for 14 h. A white solid precipitated during this time. The mixture was filtered and the volume of the green filtrate reduced (3 mL) in vacuo. Toluene (5 mL) was added, and the solution was cooled to −20 °C to produce green needles. The crystals were isolated by removing the supernatant via a cannula and dried under vacuum. With the aid of a microscope, a small amount of NaBr/$[NEt_4]Br$ was seen among the crystals of the first crop. Two recrystallizations were necessary to remove these contaminants. Anal. Calcd for $C_{18}H_{42}NO_2Re$: C, 44.06; H, 8.63; N, 2.85. Found: C, 43.96; H, 8.51; N, 2.92. ^{1}H NMR (CD_3CN): δ 3.24 (s, 4, CH_2CMe_3), 3.17 (q, 8, J_{HH} = 7.3 Hz, CH_2CH_3), 1.20 (tt, 12, J_{NH} = 2.0 Hz, J_{HH} = 7.3 Hz, CH_2CH_3), 0.93 (s, 18, CH_2CMe_3). ^{13}C{^{1}H} NMR (CD_3CN): δ 53.22 (s, CH_2CH_3), 38.03 (s, CH_2CMe_3), 35.21 (s, CH_2CMe_3), 33.88 (s, CH_2CMe_3), 7.82 (s, CH_2CH_3). IR (Nujol, CsI, cm^{-1}): ν(Re=O) = 939 s and 870 s (ν(Re=^{18}O) = 889 and 839); 1404 m, 1353 s, 1309 m, 1234 m, 1184 s, 1120 w, 1079 w, 1035 m, 1008 m, 906 m, 804 m, sh, 793 m, 648 w, 456 w, 329 w, 289 w.

$[NEt_4][Re^{18}O_2(CH_2CMe_3)_2]$. This complex was prepared by stirring $[NEt_4][ReO_2(CH_2CMe_3)_2]$ with 100 equiv of $^{18}OH_2$ in tetrahydrofuran for 18 h.

Crystallography. General operating procedures and listings of programs used at the Indiana University Molecular Structure Center have been described.[5] Crystal data are summarized in Table I.

(4) Schmidt, H.; Schmidbauer, H. *Chem. Ber.* **1959**, *92*, 2667; *Inorg. Synth.* **1967**, *9*, 149.

(5) Chisholm, M. H.; Folting, K.; Huffman, J. C.; Kirkpatrick, C. C. *Inorg. Chem.* **1984**, *23*, 1021.

$[Re_2(\mu\text{-}O)_2O_2(CH_2CMe_3)_4]$. Because of severe absorption problems, the structure of this molecule was solved for three different crystals, once at Harvard University and twice at Indiana University. The account given here is for the best analysis (IU). A suitable crystal was located and transferred to the goniostat under an inert atmosphere. It was then cooled to −155 °C for characterization and data collection. A systematic search of a limited hemisphere of reciprocal space located a set of diffraction maxima with orthorhombic symmetry and systematic absences corresponding to the space groups *Pmnb* or $P2_1nb$. Subsequent solution and refinement of the structure confirmed the noncentrosymmetric choice of $P2_1nb$ (a nonstandard setting of $Pna2_1$).

Data were collected by using a θ–2θ scan technique with fixed backgrounds. The data were corrected for absorption by using analytical techniques. Averaging for equivalent data before and after the absorption correction indicated the procedure significantly improved the data. The structure was solved by a combination of direct methods (MULTAN78) and Fourier techniques and refined by full-matrix least squares. Anisotropic refinement for all non-hydrogen atoms resulted in nonpositive definite thermal parameters for four atoms. A trial refinement with anisotropic parameters for the Re atoms and isotropic parameters for the carbon and oxygen atoms resulted in only a slightly higher residual than for a full anisotropic refinement (0.052 versus 0.049); therefore, final refinement was undertaken with isotropic parameters for carbon and oxygen and anisotropic parameters for rhenium. Hydrogen atoms were included as idealized fixed-atom contributors in the final cycles of refinement.

A final difference Fourier indicated two peaks, one at each rhenium site, of 1.3 e Å^{-3}. All remaining peaks were less than 1.0 e Å^{-3}.

$\{[Li(CH_3CN)_2][ReO_2(CH_2CMe_3)_2]\}_2$. A crystal for the structure determination was chosen from a batch that had been left slightly wet with acetonitrile. Data were collected and the structure solved in a manner similar to that described above. All non-hydrogen atoms were refined anisotropically. Many of the hydrogen atoms were visible in a difference Fourier phased on the non-hydrogen atoms. All hydrogen atom positions were calculated by assuming idealized geometries (C–H = 0.95 Å), and the hydrogen atoms were included as fixed-atom contributors in the final cycles of refinement.

A final difference Fourier was essentially featureless with the largest peak located at the rhenium (1.3 e/Å^3) and all other peaks less than 0.6 e/Å^3. The largest deviation for ψ scans of several reflections near χ = 90° was ~8%; therefore, no absorption correction was deemed necessary.

$[NEt_4][ReO_2(CH_2CMe_3)_2]$. Data were collected and the structure solved by a procedure similar to that described above. All non-hydrogen atoms were refined anisotropically. The positions of all hydrogen atoms were clearly visible in a difference Fourier phased on the non-hydrogen atoms; therefore, the coordinates and isotropic thermal parameters for the hydrogen atoms were varied in the final cycles of the refinement. A final difference Fourier was essentially featureless; the largest peak was 1.3 e Å^{-3} at the rhenium position, and all other peaks were less than 0.6 e Å^{-3}. No absorption correction was deemed necessary.

The atom-numbering scheme used in Table VI for $[NEt_4]^+$ is given in I.

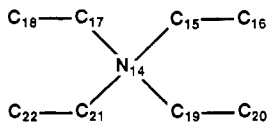

I

Results and Discussion

Synthesis and Structure of $[Re_2(\mu\text{-}O)_2O_2(CH_2CMe_3)_4]$. We have previously used the orange-red complex $[Re_2(\mu\text{-}O)O_2(CH_2SiMe_3)_6]$, prepared by reaction 1, as a starting material for various reactions.[6,7] We were interested in preparing the neopentyl-ligand complex and therefore carried out the reaction between $[Re(OSiMe_3)O_3]$ and 3 equiv of $Al(CH_2CMe_3)_3(THF)$ in hexane solvent by analogy with reaction 1. Column chromatography of the reaction mixture under N_2 on Al_2O_3 (hexane eluant) and cooling of the collected yellow band at −80 °C yielded only yellow needles of $[Re_2(\mu\text{-}O)_2O_2(CH_2CMe_3)_4]$ (**1**) in 10–20% yield. Further study revealed that the yields of **1** are optimum (43%) when 1.5 equiv of the aluminum reagent is used. An alternative alkylating agent is $Zn(CH_2CMe_3)_2$, but the yields are only 25%.

$$[Re(OSiMe_3)O_3] + 3Al(CH_2SiMe_3) \rightarrow [Re_2(\mu\text{-}O)O_2(CH_2SiMe_3)_6] \quad (1)$$

It is unclear why the $[Re_2(\mu\text{-}O)O_2R_6]$ complex is not the major product of the reaction between $[Re(OSiMe_3)O_3]$ and AlR_3, R = CH_2CMe_3, as it is for reactions where R = Me or CH_2SiMe_3.[2,6] We do see variable but minor amounts of oily $[Re_2(\mu\text{-}O)_2O_2(CH_2SiMe_3)_4]$ formed in reaction 1, but reactions employing $AlMe_3$, carried out under similar conditions, are reported to be very clean for formation of $[Re_2(\mu\text{-}O)O_2Me_6]$.[2] We can rule out the possibility that we destroy $[Re_2(\mu\text{-}O)O_2(CH_2CMe_3)_6]$ during workup since we have monitored the $Al(CH_2CMe_3)_3$ reaction by ^1H NMR and see no evidence for $[Re_2(\mu\text{-}O)O_2(CH_2CMe_3)_6]$ formation during the course of the reaction. Also, $[Re_2(\mu\text{-}O)_2O_2(CH_2CMe_3)_4]$ does not react further with $Al(CH_2CMe_3)_3$ and is therefore probably not an intermediate in the reaction to form $[Re_2(\mu\text{-}O)O_2(CH_2CMe_3)_6]$. Obviously, these reactions are complicated and subtle changes in conditions and ligand set greatly affect the product distribution.

Table II. Selected Bond Distances (Å) and Angles (deg) for $[Re_2(\mu\text{-}O)_2O_2(CH_2CMe_3)_4]$ (**1**)[a]

Bond Distances			
Re(1)–Re(2)	2.606 (1)	Re(2)–O(6)	1.861 (18)
Re(1)–O(3)	1.657 (18)	Re(2)–C(17)	2.21 (3)
Re(1)–O(5)	1.946 (18)	Re(2)–C(22)	2.148 (28)
Re(1)–O(6)	1.967 (17)	C(7)–C(8)	1.53 (3)
Re(1)–C(7)	2.163 (26)	C(12)–C(13)	1.56 (4)
Re(1)–C(12)	2.149 (27)	C(17)–C(18)	1.51 (4)
Re(2)–O(4)	1.626 (14)	C(22)–C(23)	1.52 (4)
Re(2)–O(5)	1.977 (18)		

Bond Angles			
O(3)–Re(1)–O(5)	118.8 (8)	O(4)–Re(2)–O(6)	128.5 (9)
O(3)–Re(1)–O(6)	120.3 (8)	O(4)–Re(2)–C(17)	103.2 (10)
O(3)–Re(1)–C(7)	106.6 (9)	O(4)–Re(2)–C(22)	99.2 (9)
O(3)–Re(1)–C(12)	99.3 (9)	O(5)–Re(2)–O(6)	88.1 (7)
O(5)–Re(1)–O(6)	86.1 (7)	O(5)–Re(2)–C(17)	75.1 (9)
O(5)–Re(1)–C(7)	133.2 (9)	O(5)–Re(2)–C(22)	142.0 (9)
O(5)–Re(1)–C(12)	81.6 (10)	O(6)–Re(2)–C(17)	127.6 (9)
O(6)–Re(1)–C(7)	80.6 (9)	O(6)–Re(2)–C(22)	82.3 (9)
O(6)–Re(1)–C(12)	139.5 (9)	C(17)–Re(2)–C(22)	81.9 (11)
C(7)–Re(1)–C(12)	80.3 (10)	Re(1)–C(7)–C(8)	116.5 (18)
O(4)–Re(2)–O(5)	115.1 (8)	Re(1)–C(12)–C(13)	122.8 (18)
Re(1)–O(5)–Re(2)	83.3 (7)	Re(2)–C(22)–C(23)	122.9 (19)
Re(1)–O(6)–Re(2)	85.8 (7)	Re(2)–C(17)–C(18)	117.5 (19)

Dihedral Angle	
O(3)–Re(1)–Re(2)–O(4)	8.1 (1.0)

Angles between Planes	
Re(1), O(5), O(6) and Re(2), O(5), O(6)	136
O(5), O(6), C(7), C(12) and O(5), O(6), C(17), C(22)	157

[a] A complete table of bond distances and angles is given in the supplementary material.

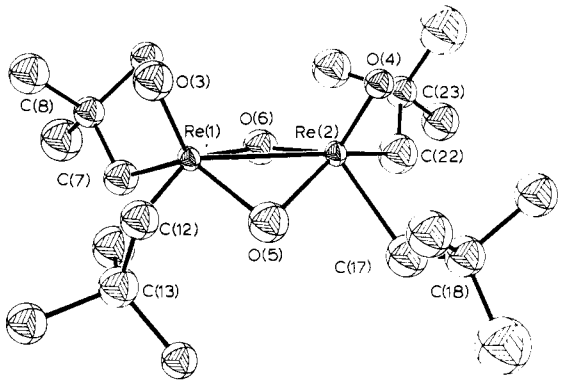

Figure 1. ORTEP drawing of $[Re_2(\mu\text{-}O)_2O_2(CH_2CMe_3)_4]$ (**1**) showing the atom-numbering scheme used in the tables. A ball and stick drawing showing the complete atom-numbering scheme is given in the supplementary material.

(6) Cai, S.; Hoffman, D. M.; Lappas, D.; Woo, H.-G. *Organometallics*, in press.

(7) The complex $[Re_2(\mu\text{-}O)O_2(CH_2SiMe_3)_6]$ has been prepared by at least two other methods. See ref 2 and: Mertis, K.; Williamson, D. H.; Wilkinson, G. *J. Chem. Soc., Dalton Trans.* **1975**, 607.

Table III. Fractional Coordinates for Selected Non-Hydrogen Atoms of $[Re_2(\mu\text{-}O)_2O_2(CH_2CMe_3)_4]$ (**1**)[a,b]

atom	x	y	z
Re(1)	−1686 (1)	−5733.5 (4)	209 (2)
Re(2)	−1272[c]	−6816.3 (4)	−1514 (2)
O(3)	8069 (8)	4769 (9)	8208 (32)
O(4)	−1212 (10)	−6819 (7)	−4244 (24)
O(5)	−813 (9)	−6100 (9)	19 (31)
O(6)	−1999 (9)	−6632 (8)	252 (31)
C(7)	−2392 (12)	−5662 (13)	2906 (46)
C(8)	−3098 (12)	−5521 (12)	2214 (44)
C(12)	−1190 (15)	−5059 (12)	2363 (44)
C(13)	−507 (13)	−4769 (13)	1779 (46)
C(17)	−331 (14)	−7235 (14)	−405 (50)
C(18)	226 (13)	−7225 (13)	−2059 (47)
C(22)	−1596 (15)	−7792 (13)	−1006 (46)
C(23)	−2226 (12)	−8052 (12)	−1993 (46)

[a] Fractional coordinates are $\times 10^4$. [b] A complete table of positional parameters is given in the supplementary material. [c] Not varied.

The structure of $[Re_2(\mu\text{-}O)_2O_2(CH_2CMe_3)_4]$ as determined from an X-ray diffraction study is shown by the ORTEP drawing in figure 1. In Tables II and III are given selected bond distances and angles and the final fractional coordinates, respectively. The structure of $[Re_2(\mu\text{-}O)_2O_2(CH_2CMe_3)_4]$ consists of two approximately square pyramidal Re centers linked by bridging oxo ligands. At each Re center the two bridging oxo ligands and two terminal alkyl ligands define the square plane and another oxo ligand occupies the apical position. The Re atoms are displaced from the square planes by 0.76 Å (average) in the direction of the apical oxygen atoms. The Re–C and terminal and bridging Re–O bond distances are normal,[2,6,8] and the Re–Re distance of 2.606 (2) Å is short for a single bond but is within the range of distances observed previously.[1]

Overall the structure of $[Re_2(\mu\text{-}O)_2O_2(CH_2CMe_3)_4]$ is very similar to that of $[Re_2(\mu\text{-}O)_2O_2(CH_2CMe_2Ph)_4]$, reported while this paper was in preparation.[9] It appears to be the only other example of a rhenium d^1–d^1 $[M_2(\mu\text{-}O)_2O_2]$-type complex. However, there are many examples of molybdenum complexes with the same structural core, and the most closely related to the rhenium complex are $[Mo_2(\mu\text{-}O)_2O_2(S_2CNEt_2)_2]$ and $[Mo_2(\mu\text{-}O)_2O_2Cl_4]^{2-}$.[10] Both have square-pyramidal metal centers joined at an edge with Mo–Mo = 2.58 and 2.59 Å, respectively.

Table IV. Bond Distances (Å) and Angles (deg) for $\{[Li(CH_3CN)_2][ReO_2(CH_2CMe_3)_2]\}_2$ (**2a**)

Bond Distances			
Re(1)–O(2)	1.749 (9)	C(4)–C(5)	1.545 (19)
Re(1)–O(3)	1.739 (8)	C(5)–C(6)	1.542 (20)
Re(1)–C(4)	2.108 (14)	C(5)–C(7)	1.544 (19)
Re(1)–C(9)	2.106 (12)	C(5)–C(8)	1.537 (21)
O(2)–Li(20)	1.893 (26)	C(9)–C(10)	1.541 (18)
O(3)–Li(20)	1.892 (24)	C(10)–C(11)	1.546 (19)
N(14)–C(15)	1.116 (15)	C(10)–C(12)	1.534 (18)
N(14)–Li(20)	2.059 (26)	C(10)–C(13)	1.498 (19)
N(17)–C(18)	1.140 (16)	C(15)–C(16)	1.461 (20)
N(17)–Li(20)	2.140 (26)	C(18)–C(19)	1.414 (20)
Bond Angles			
O(2)–Re(1)–O(3)	134.9 (4)	C(7)–C(5)–C(8)	108.9 (12)
O(2)–Re(1)–C(4)	106.9 (5)	Re(1)–C(9)–C(10)	119.6 (8)
O(2)–Re(1)–C(9)	107.9 (4)	C(9)–C(10)–C(11)	109.7 (11)
O(3)–Re(1)–C(4)	106.0 (5)	C(9)–C(10)–C(12)	109.0 (11)
O(3)–Re(1)–C(9)	105.6 (4)	C(9)–C(10)–C(13)	111.6 (10)
C(4)–Re(1)–C(9)	83.7 (5)	C(11)–C(10)–C(12)	107.8 (11)
Re(1)–O(2)–Li(20)	165.3 (9)	C(11)–C(10)–C(13)	108.0 (12)
Re(1)–O(3)–Li(20)	125.2 (9)	C(12)–C(10)–C(13)	110.6 (12)
C(15)–N(14)–Li(20)	156.4 (13)	N(14)–C(15)–C(16)	177.8 (15)
C(18)–N(17)–Li(20)	146.2 (13)	N(17)–C(18)–C(19)	179.2 (16)
Re(1)–C(4)–C(5)	119.1 (9)	O(2)–Li(20)–O(3)	111.4 (12)
C(4)–C(5)–C(6)	108.6 (12)	O(2)–Li(20)–N(14)	106.2 (12)
C(4)–C(5)–C(7)	108.5 (11)	O(2)–Li(20)–N(17)	103.8 (11)
C(4)–C(5)–C(8)	112.1 (11)	O(3)–Li(20)–N(14)	110.0 (11)
C(6)–C(5)–C(7)	108.0 (11)	O(3)–Li(20)–N(17)	105.7 (12)
C(6)–C(5)–C(8)	110.7 (12)	N(14)–Li(20)–N(17)	119.6 (12)

The ^1H NMR spectrum for $[Re_2(\mu\text{-}O)_2O_2(CH_2CMe_3)_4]$ is consistent with the solid-state molecular structure and shows one AB quartet in the methylene region and a singlet in the methyl region. The proton-decoupled and -coupled ^{13}C NMR spectra are also consistent with the solid-state structure, in the former case revealing only singlets for the methylene, quaternary, and methyl carbon atoms.

Infrared spectra were recorded for KBr pellets of $[Re_2(\mu\text{-}O)_2O_2(CH_2CMe_3)_4]$ and the corresponding oxygen-18 complex (**1**-^{18}O). The labeled compound was prepared by stirring $[Re_2(\mu\text{-}O)_2O_2(CH_2CMe_3)_4]$ with excess $^{18}OH_2$ in tetrahydrofuran solvent. In general, the C_{2v} $[M_2(\mu\text{-}O)_2O_2]$ moiety should give rise to five IR-active bands, two associated with the terminal M=O bonds and three with the $[M_2(\mu\text{-}O)_2]$ moiety.[10b,11] However, only two of the three $[M_2(\mu\text{-}O)_2]$ bands are normally observed, and this is the case for $[Re_2(\mu\text{-}O)_2O_2(CH_2CMe_3)_4]$. Two strong bands in the IR spectrum of **1** at 1027 and 1013 cm^{-1} shift to 966 (calculated 973) and 957 (calculated 960) cm^{-1} for **1**-^{18}O and can be assigned to terminal Re—O stretches. One band of medium intensity at 755 cm^{-1} that shifts to 708 (calculated 715) cm^{-1} for **1**-^{18}O can be assigned to a $[Re_2(\mu\text{-}O)_2]$ stretch. A second IR band associated with the $[Re_2(\mu\text{-}O)_2]$ moiety is assigned to a weak-intensity band observed at 514 cm^{-1} that shifts to 496 (calculated 487) cm^{-1} for **1**-^{18}O. We are not certain why this band shifts only 67% of the calculated value since the same bands for the analogous Mo compounds, $[Mo_2(\mu\text{-}O)_2O_2(S_2CNR_2)_2]$, do shift approximately the theoretical amount.[11a]

Synthesis of $[ReO_2(CH_2CMe_3)_2]^-$ Complexes. Literature reports of d^2–d^2 $[M_2(\mu\text{-}O)_2O_2]$ complexes with and without M–M bonds,[12] coupled with the general notion that anionic oxo complexes should show enhanced reactivity toward electrophiles, prompted us to attempt the reduction of $[Re_2(\mu\text{-}O)_2O_2(CH_2CMe_3)_4]$.

Reduction of $[Re_2(\mu\text{-}O)_2O_2(CH_2CMe_3)_4]$ in pentane with 6 equiv of Li/Hg (0.014%) or 2 equiv of Na/Hg (0.02%) results in deposition of a green solid. Removing the pentane in vacuo,

(8) (a) Ciani, G.; Sironi, A.; Beringhelli, T.; D'Alfonso, G.; Freni, M. *Inorg. Chim. Acta* **1986**, *113*, 61. Blower, P. J.; Dilworth, J. R.; Hutchinson, J.; Nicholson, T.; Zubieta, J. *Ibid.* **1984**, *90*, L27. Ciani, G. F.; D'Alfonso, G.; Romiti, P.; Sironi, A.; Freni, M. *Ibid.* **1983**, *72*, 29. Carrondo, M.; Middleton, A. R.; Skapski, A. C.; West, A. P.; Wilkinson, G. *Ibid.* **1980**, *44*, L7. Lis, T.; Jezowska-Trzebiatowska, B. *Acta Crystallogr., Sect. B: Struct. Crystallogr. Cryst. Chem.* **1977**, *B33*, 1248. Gilli, G.; Sacerdoti, M.; Bertolasi, V.; Rossi, R. *Ibid.* **1982**, *B38*, 100. Krebs, B.; Hasse, K.-D. *Ibid.* **1976**, *B32*, 1334. Lis, T. *Ibid.* **1979**, *B35*, 3041, 1230. Lock, C. J. L.; Turner, G. *Can. J. Chem.* **1977**, *55*, 333; **1978**, *56*, 179. Lock, C. J. L.; Wan, C. *Ibid.* **1975**, *53*, 1548. McDonell, A. C.; Hambley, T. W.; Snow, M. R.; Wedd, A. G. *Aust. J. Chem.* **1983**, *36*, 253. Shandles, R.; Schlemper, E. O.; Murmann, R. K. *Inorg. Chem.* **1971**, *10*, 2785. Tisley, D. G.; Walton, R. A.; Wills, D. L. *Inorg. Nucl. Chem. Lett.* **1971**, *7*, 523. Fletcher, S. R.; Rowbottom, J. F.; Skapski, A. C.; Wilkinson, G. *J. Chem. Soc. D* **1970**, 1572. Chiu, K. W.; Wong, W.-K.; Wilkinson, G.; Galas, A. M. R.; Hursthouse, M. B. *J. Chem. Soc., Chem. Commun.* **1982**, 31. Hursthouse, M. B.; Jayaweera, S. A.; Quick, A. *J. Chem. Soc., Dalton Trans.* **1979**, 279. Edwards, P. G.; Wilkinson, G.; Hursthouse, M. B.; Malik, K. M. A. *Ibid.* **1980**, 2467. Mayer, J. M.; Thorn, D. L.; Tulip, T. H. *J. Am. Chem. Soc.* **1985**, *107*, 7454. (b) Edwards, P. G.; Skapski, A. C.; Slawin, A. M.; Wilkinson, G. *Polyhedron* **1984**, *3*, 1083. Calvo, C.; Krishnamachari, N.; Lock, C. J. L. *J. Cryst. Mol. Struct.* **1971**, *1*, 161. Murmann, R. K.; Schlemper, E. O. *Inorg. Chem.* **1971**, *10*, 2352. Lock, C. J. L.; Turner, G. *Acta Crsytallogr., Sect. B: Struct. Crystallogr. Cryst. Chem.* **1978**, *B34*, 923.

(9) Huggins, J. M.; Whitt, D. R.; Lebioda, L. *J. Organomet. Chem.* **1986**, *312*, C15.

(10) (a) Ricard, L.; Martin, C.; Wiest, R.; Weiss, R. *Inorg. Chem.* **1975**, *14*, 2300. Moynihan, K. J.; Boorman, P. M.; Ball, J. M.; Patel, V. D.; Kerr, K. A. *Acta Crystallogr., Sect. B: Struct. Crystallogr. Cryst. Chem.* **1982**, *B38*, 2258. (b) A general discussion of the structure type can be found in: Stiefel, E. I. *Prog. Inorg. Chem.* **1977**, *22*, 1–224.

(11) (a) Newton, W. E.; McDonald, J. W. *J. Less-Common Met.* **1977**, *54*, 51. (b) Jezowska-Trzebiatowska, B.; Rudolf, M. F.; Natkaniec, L.; Sabat, H. *Inorg. Chem.* **1974**, *13*, 617. Wing, R. M.; Callahan, K. P. *Inorg. Chem.* **1969**, *8*, 871.

(12) $[(\eta^5\text{-}C_5Me_5)_2Re_2O_2(\mu\text{-}O)_2]$ (Re=Re): Herrmann, W. A.; Serrano, R.; Kusthardt, U.; Ziegler, M. L.; Guggolz, E.; Zahn, T. *Angew. Chem., Int. Ed. Engl.* **1984**, *23*, 515; *Angew. Chem.* **1984**, *96*, 498. $\{[OsO_2(O_2C_2Me_2)]\}_2$: Phillips, F. L.; Skapski, A. C. *J. Chem. Soc., Dalton Trans.* **1975**, 2586.

Table V. Fractional Coordinates for the Non-Hydrogen Atoms of $\{[Li(CH_3CN)_2][ReO_2(CH_2CMe_3)_2]\}_2$ (**2a**)[a]

atom	*x*	*y*	*z*
Re(1)	1524.2 (4)	621.4 (3)	1383 (1)
O(2)	815 (7)	−198 (5)	1829 (9)
O(3)	1422 (7)	1133 (5)	−193 (8)
C(4)	1648 (11)	1510 (8)	2949 (14)
C(5)	702 (13)	2156 (8)	2673 (15)
C(6)	822 (14)	2590 (9)	4097 (15)
C(7)	895 (12)	2779 (9)	1611 (16)
C(8)	−504 (13)	1797 (9)	2038 (17)
C(9)	3292 (11)	481 (7)	2450 (12)
C(10)	3921 (11)	−259 (8)	2134 (13)
C(11)	3665 (13)	−347 (10)	497 (17)
C(12)	5217 (11)	−137 (9)	2814 (15)
C(13)	3546 (14)	−1015 (9)	2678 (19)
N(14)	−1019 (10)	−479 (7)	3415 (11)
C(15)	8619 (10)	0 (8)	3936 (14)
C(16)	−1867 (11)	604 (9)	4651 (14)
N(17)	660 (10)	−2052 (7)	2492 (12)
C(18)	1278 (11)	−2480 (8)	2205 (14)
C(19)	2048 (14)	−3014 (9)	1871 (20)
Li(20)	−285 (19)	−955 (15)	1983 (25)

[a] Fractional coordinates are ×10⁴.

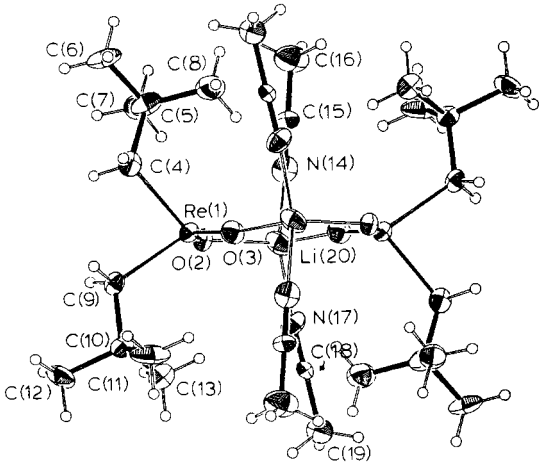

Figure 2. ORTEP drawing of $\{[Li(CH_3CN)_2][ReO_2(CH_2CMe_3)_2]\}_2$ (**2a**) showing the atom-numbering scheme used in the tables.

dissolving the green residue in CH_3CN, and filtering gives a clear green solution from which the air-sensitive green compounds $M[ReO_2(CH_2CMe_3)_2]$, M = Li (**2a**) and Na (**2b**), may be isolated. The lithium salt can also be prepared by reaction of $[Re_2(\mu\text{-}O)_2O_2(CH_2CMe_3)_4]$ with *n*-BuLi in hexane. The salt $[NEt_4][ReO_2(CH_2CMe_3)_2]$ (**2c**) was prepared by cation exchange involving the Na salt. Oxidation of the compounds with $AgBF_4$ produces the starting material $[Re_2(\mu\text{-}O)_2O_2(CH_2CMe_3)_4]$ quantitatively.

The compounds **2a–c** are insoluble in hydrocarbon solvents, and **2a** and **2b** lose acetonitrile from their crystalline forms under vacuum. As shown by an X-ray crystallographic study, **2a** is properly formulated in the crystalline form as $\{[Li(CH_3CN)_2][ReO_2(CH_2CMe_3)_2]\}_2$. Analysis of NMR spectra for inert-gas-dried crystals of the sodium salt also showed the presence of two acetonitrile molecules per anion, and we therefore formulate the salt as $\{[Na(CH_3CN)_2][ReO_2(CH_2CMe_3)_2]\}_x$.

Chemical analyses for **2a** that had been held under vacuum for >12 h to remove the solvent of crystallization were variable but did indicate that most of the acetonitrile was removed. The combustion analysis of a similarly treated sample of **2b** was excellent and showed that all of the solvent of crystallization was removed. With the assumption of the complete removal of solvent under vacuum for **2a**, the isolated yields of the salts are 66% (**2a**) and 75% (**2b**). The yield of the lithium salt from the reaction employing *n*-BuLi as a reducing agent is 20%.

Structure of $[ReO_2(CH_2CMe_3)_2]^-$ Complexes. As explained below, analysis of the NMR and IR spectra for **2a–c** indicated the $[ReO_2(CH_2CMe_3)_2]^-$ formulation was correct. However, since the compounds were found to be diamagnetic, it was felt that they should be distorted, and we undertook a single-crystal X-ray diffraction study of the lithium salt in order to confirm this expectation. Analysis of the structure left questions concerning the role the Li^+ played in determining the geometry of the anion, and therefore another study was undertaken for the $[NEt_4]^+$ salt.

In Tables IV and VI selected bond distances and angles, in Tables V and VII final fractional coordinates, and in Figures 2

Table VI. Bond Distances (Å) and Angles (deg) for $[NEt_4][ReO_2(CH_2CMe_3)_2]$ (**2c**)

Bond Distances			
Re(1)–O(2)	1.732 (8)	C(10)–C(12)	1.549 (16)
Re(1)–O(3)	1.733 (8)	C(10)–C(13)	1.504 (18)
Re(1)–C(4)	2.107 (12)	N(14)–C(15)	1.511 (15)
Re(1)–C(9)	2.099 (11)	N(14)–C(17)	1.506 (14)
C(4)–C(5)	1.545 (18)	N(14)–C(19)	1.502 (15)
C(5)–C(6)	1.515 (18)	N(14)–C(21)	1.502 (14)
C(5)–C(7)	1.542 (18)	C(15)–C(16)	1.508 (18)
C(5)–C(8)	1.537 (17)	C(17)–C(18)	1.502 (18)
C(9)–C(10)	1.560 (16)	C(19)–C(20)	1.529 (19)
C(10)–C(11)	1.522 (19)	C(21)–C(22)	1.502 (18)
Bond Angles			
O(2)–Re(1)–O(3)	127.5 (4)	C(9)–C(10)–C(12)	107.8 (9)
O(2)–Re(1)–C(4)	110.5 (5)	C(9)–C(10)–C(13)	110.0 (11)
O(2)–Re(1)–C(9)	107.8 (4)	C(11)–C(10)–C(12)	109.8 (11)
O(3)–Re(1)–C(4)	108.9 (5)	C(11)–C(10)–C(13)	109.6 (12)
O(3)–Re(1)–C(9)	111.2 (4)	C(12)–C(10)–C(13)	109.8 (11)
C(4)–Re(1)–C(9)	81.2 (5)	N(14)–C(15)–C(16)	114.4 (10)
Re(1)–C(4)–C(5)	121.6 (9)	N(14)–C(17)–C(18)	116.7 (11)
C(4)–C(5)–C(6)	109.0 (10)	N(14)–C(19)–C(20)	116.4 (10)
C(4)–C(5)–C(7)	109.0 (10)	N(14)–C(21)–C(22)	117.4 (11)
C(4)–C(5)–C(8)	110.7 (11)	C(15)–N(14)–C(17)	108.2 (8)
C(6)–C(5)–C(7)	110.6 (11)	C(15)–N(14)–C(19)	112.2 (9)
C(6)–C(5)–C(8)	107.9 (11)	C(15)–N(14)–C(21)	107.4 (9)
C(7)–C(5)–C(8)	109.7 (11)	C(17)–N(14)–C(19)	109.6 (9)
Re(1)–C(9)–C(10)	120.6 (8)	C(17)–N(14)–C(21)	111.2 (9)
C(9)–C(10)–C(11)	109.8 (10)	C(19)–N(14)–C(21)	108.3 (9)

Selected Nonbonded Distances			
$O(2)\cdots C(19)H_2$[a]	3.23	$O(2)\cdots C(17)H_2$[a]	3.32
$O(3)\cdots C(15)H_2$[a]	3.27	$H_3C(6)\cdots C(16)H_3$[b]	3.88
$H_3C(6)\cdots C(16)H_3$[b]	3.88	$H_3C(12)\cdots C(16)H_3$[b]	3.89
$H_3C(13)\cdots C(22)H_3$[b]	3.94		

[a] Distance to $[NEt_4]^+$ within the asymmetric unit. The sum of the van der Waals radii for oxygen and methylene/methyl is 3.4 Å. The sum of the van der Waals radii for two methyl groups is 4.0 Å. [b] Distance to $[NEt_4]^+$ in the adjacent asymmetric unit.

Table VII. Fractional Coordinates for the Non-Hydorgen Atoms of $[NEt_4][ReO_2(CH_2CMe_3)_2]$[a]

atom	*x*	*y*	*z*
Re(1)	7269.5 (4)	1302.3 (2)	8411.3 (4)
O(2)	8747 (8)	934 (4)	9037 (7)
O(3)	5625 (8)	1074 (4)	8562 (8)
C(4)	7396 (12)	1578 (6)	6511 (11)
C(5)	7618 (12)	1094 (6)	5464 (11)
C(6)	7479 (14)	1423 (6)	4182 (12)
C(7)	9037 (13)	804 (6)	5755 (12)
C(8)	6545 (13)	573 (6)	5410 (13)
C(9)	7523 (11)	2273 (5)	8705 (10)
C(10)	7430 (11)	2566 (5)	10047 (12)
C(11)	8485 (13)	2270 (7)	11020 (12)
C(12)	5997 (12)	2431 (6)	10419 (12)
C(13)	7659 (14)	3265 (6)	10002 (14)
N(14)	2424 (9)	913 (4)	307 (9)
C(15)	2818 (11)	1505 (5)	−354 (11)
C(16)	1689 (13)	1798 (6)	−1229 (12)
C(17)	1412 (11)	1088 (5)	1205 (11)
C(18)	1064 (13)	589 (6)	2120 (11)
C(19)	1825 (10)	427 (5)	−620 (11)
C(20)	2679 (13)	235 (7)	−1673 (13)
C(21)	3687 (11)	646 (6)	1018 (11)
C(22)	4354 (12)	1020 (7)	2122 (12)

[a] Fractional coordinates are ×10⁴.

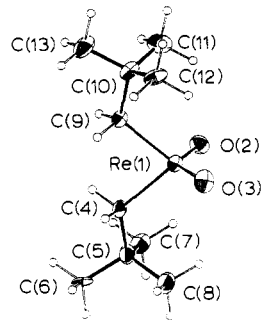

Figure 3. ORTEP drawing of the anion of $[NEt_4][ReO_2(CH_2CMe_3)_2]$ (**2c**) showing the atom-numbering scheme used in the tables. The atom-numbering scheme for the cation is given in the Experimental Section.

and 3 ORTEP views are given for **2a** and **2c**, respectively. For brevity we will discuss the structures of **2a** and **2c** together as much as possible. In the crystalline form, **2a** is the dimer $\{[Li(CH_3CN)_2][ReO_2(CH_2CMe_3)_2]\}_2$, with the halves related by an inversion center. The structure consists of two four-coordinate $[ReO_2(CH_2CMe_3)_2]^-$ anions linked via two bridging $[Li(CH_3CN)_2]^+$ cations coordinated to the oxygens of the Re–O bonds to form an eight-membered ring. The eight-membered ring is nearly planar with one Li^+ cation lying 0.13 Å above and another 0.13 Å below the plane defined by the two Re and four oxygen atoms (maximum deviations for the plane are ±0.09 (1) Å for O(3) and O(3)′).

The structure of **2c** consists of four-coordinate $[ReO_2(CH_2CMe_3)_2]^-$ anions and $[NEt_4]^+$ cations. In Table VI are listed several interion nonbonded distances between the oxo ligands of the anion and methylene groups of the cation that are slightly less than the sum of the van der Waals radii of 3.4 Å;[13] however, we do not regard these as significant and will discuss the anion as a discrete species. The structure of the cation is unexceptional and will not be discussed further.

The Re—C and Re=O bond distances in **2a** and **2c** are the same within experimental error and are within the range of values observed previously.[2,6,8,9] The equivalence of the Re=O distances indicates that the Re=O bonds in **2a** are not significantly perturbed by coordination to $[Li(CH_3CN)_2]^+$. The closest intramolecular nonbonded distances of interest in **2a** and **2c** involve one hydrogen from each neopentyl ligand and the oxo ligands, but in neither case was the distance less that the sum of the van der Waals radii.[13]

As anticipated, the anions are angularly distorted from a tetrahedral geometry. The O(2)–Re–O(3) angles are 134.9 (4) and 127.5 (4)° and the C(4)–Re–C(9) angles are 83.7 (5) and 81.2 (5)° for **2a** and **2c**, respectively. The distortion is with retention of a C_{2v} $[ReO_2C_2]$-core symmetry since the angles between the planes defined by O(2)–Re–O(3) and C(4)–Re–C(9) are within experimental error of 90° (90.5 (5) (**2a**) and 92.0 (1.5)° (**2c**)).

Overall, the structures of $[ReO_2(CH_2CMe_3)_2]^-$ in **2a** and **2c** are very similar with the exception of the 7° larger O–Re–O angle for the **2a** anion. We attribute that difference to the ring structure of the lithium salt that forces an opening of the angle. It is also interesting that the smaller O–Re–O angle in $[NEt_4][ReO_2(CH_2CMe_3)_2]$ is concomitant with a slightly smaller C–Re–C angle.

The structures of $[ReO_2(CH_2CMe_3)_2]^-$ in **2a** and **2c** are unprecedented but can be related to a large class of d^2 compounds. It is well-known that the preferred coordination for d^2 MO_2-containing complexes is trans with octahedral coordination, e.g., $[ReO_2(py)_4]^+$.[14] The anions $[ReO_2(CH_2CMe_3)_2]^-$ in **2a** and **2c** are distorted in the direction of that geometry, but with two coordination sites unoccupied. Given this rationalization for the structures of the anions, one would predict that they should readily take up ligands to fill the empty octahedral sites. Thus far we have no evidence that this is the case, but we are actively pursuing reactivity studies of this type. A more elaborate rationalization for the structural distortions will be presented below in the context of molecular orbital calculations.

Spectroscopic Studies of $[ReO_2(CH_2CMe_3)_2]^-$. The IR spectra for **2a–c** show two bands in the region 850–950 cm^{-1} (939 and 870 cm^{-1} for $[NEt_4][ReO_2(CH_2CMe_3)_2]$) that are assigned to the symmetric and antisymmetric stretches arising from the cis-dioxo group.[15] An analysis of the IR spectrum of oxygen-18-labeled $[NEt_4][ReO_2(CH_2CMe_3)_2]$, prepared by stirring $[NEt_4][ReO_2(CH_2CMe_3)_2]$ with excess $^{18}OH_2$ in tetrahydrofuran, confirmed the assignments with bands observed at 889 (calculated 890) and 839 (calculated 824) cm^{-1}.

On the basis of the d^2 $[ReO_2(CH_2CMe_3)_2]^-$ formulation, we thought that the compounds could be paramagnetic or show a temperature-dependent paramagnetism. The ^1H NMR spectra for solvent-free samples of **2a** and **2b** recorded in acetonitrile-d_3 reveal only two singlet resonances in the integral ratio of 2:9 (δ 3.62 and 0.97, respectively, for **2a**). The resonances are sharp at room temperature and below (−20 °C), but as the temperature is raised above room temperature there is reversible broadening of the methylene resonance observed for both compounds. This is not the result of a temperature-dependent paramagnetism since no solution magnetic moment is observed at 23 °C for **2a** or **2b** and at +50 °C for **2b** by the Evans NMR method.[16] Instead, we believe that the broadening is due to reversible oligomerization in solution through cation bridges. Consistent with this hypothesis, ^1H NMR spectra recorded for acetonitrile-d_3 solutions of $[NEt_4][ReO_2(CH_2CMe_3)_2]$, a salt for which oligomerization is unlikely, are sharp in the range +23–70 °C. Furthermore, spectra recorded for **2a** dissolved in DMSO-d_6 or pyridine-d_5, solvents that should strongly solvate the cations and disfavor oligomerization, do not show the high-temperature broadening that is observed in acetonitrile-d_3.

Electrochemical Studies. As one would expect upon the basis of the chemical-redox chemistry outlined above, the cyclic voltammetric responses at a platinum electrode are similar for acetonitrile solutions of the complexes $[Re_2(\mu\text{-}O)_2O_2(CH_2CMe_3)_4]$ and $Li[ReO_2(CH_2CMe_3)_2]$. The complex $[Re_2(\mu\text{-}O)_2O_2(CH_2CMe_3)_4]$ gives rise to a well-defined reduction process at −0.64 V (versus SCE; $E_p = (E_{pc} + E_{pa})/2$), and $Li[ReO_2(CH_2CMe_3)_2]$ exhibits a well-defined oxidation process at −0.64 V, both at a scan rate of 0.05 V s^{-1}. Complex **1** also exhibits an ill-defined oxidation wave (+0.88 V) and complex **2a** can be reduced (−1.45 V) irreversibly.

In order to test for reversibility of the $[Re_2(\mu\text{-}O)_2O_2(CH_2CMe_3)_4]$ reduction process and the $[ReO_2(CH_2CMe_3)_2]^-$ oxidation process, the scan rates for cyclic voltammetric tests were varied from 0.05 to 0.50 V s^{-1}. It was found that the current ratio of the cathodic peak to the aniodic peak (i_{pc}/i_{pa}) was approximately equal to unity, the potential difference ΔE_p ($\Delta E_p = E_{pa} - E_{pc}$) slightly increased as the scan rate was increased, and ΔE_p was equal to 0.12 V, which is 4 times that for a reversible two-electron process. Since 2 mol of electrons/mol of $[Re_2(\mu\text{-}O)_2O_2(CH_2CMe_3)_4]$ is needed to produce 2 mol of $[ReO_2(CH_2CMe_3)_2]^-$, we conclude that both the reduction of $[Re_2(\mu\text{-}O)_2O_2(CH_2CMe_3)_4]$ and the oxidation of $[ReO_2(CH_2CMe_3)_2]^-$ are quasi-reversible.

Theoretical Studies. In order to understand the angular distortions of $[ReO_2(CH_2CMe_3)_2]^-$ in more detail, we have performed extended Hückel calculations.[17] The extended Hückel method has several well-known deficiencies but models angular changes well and is an appropriate method in the present case.[18] As a

(13) Pauling, L. *The Nature of the Chemical-Bond*, 3rd ed.; Cornell University Press: Ithaca, NY, 1960; pp 257–264.
(14) Cotton, F. A.; Wilkinson, G. *Advanced Inorganic Chemistry*, 4th ed.; Wiley: New York, 1980; pp 897–898. Also see ref 8b.
(15) Cotton, F. A.; Wing, R. M. *Inorg. Chem.* **1965**, *4*, 867. Nakamoto, K. *Infrared Spectra of Inorganic and Coordination Compounds*, 2nd ed.; Wiley: New York, 1970; pp 114–115. Reference 10b, pp 39–41.
(16) Live, D. H.; Chan, S. I. *Anal. Chem.* **1970**, *42*, 79.
(17) Hoffmann, R. *J. Chem. Phys.* **1963**, *39*, 1397–1412. Weighted H_{ij}'s were used: Ammeter, J. H.; Bürgi, H. B.; Thibeault, J. C.; Hoffmann, R. *J. Am. Chem. Soc.* **1978**, *100*, 3686–3692. Parameters for Re were taken from: Shaik, S.; Hoffmann, R.; Fisel, C. R.; Summerville, R. H. *J. Am. Chem. Soc.* **1980**, *102*, 4555–4572.

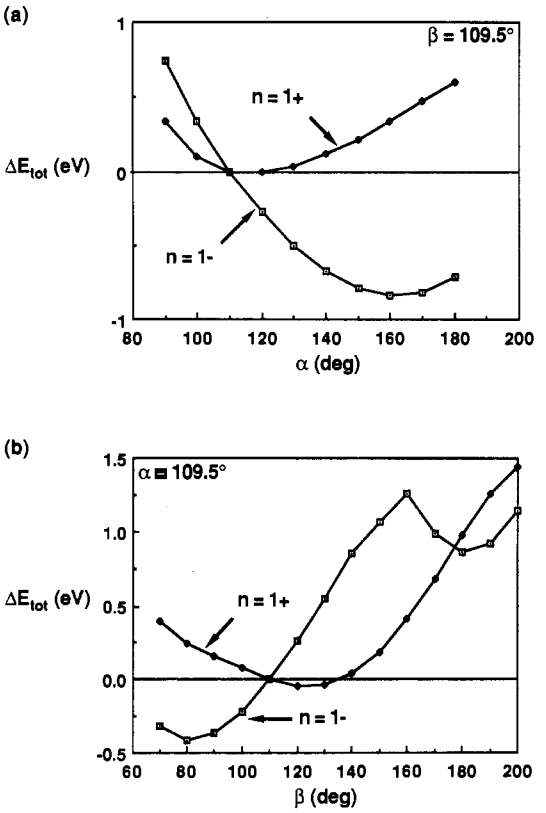

Figure 4. Relative total energy plots for (a) variation of the angle α with β = 109.5° and (b) variation of the angle β with α = 109.5° for the model system described in **3**.

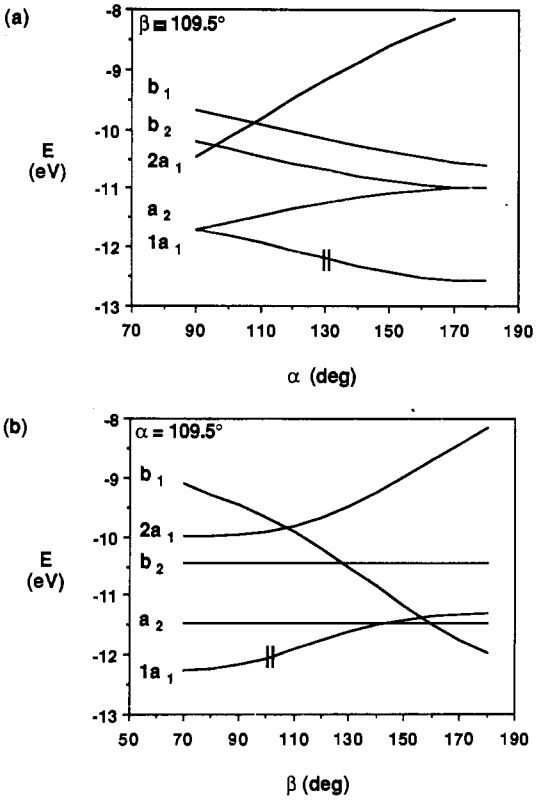

Figure 5. Walsh diagrams for $[ReO_2H_2]^-$ showing the energy changes occurring for the d-block molecular orbitals: (a) changes for variation of the angle α with β = 109.5°; (b) changes for variation of β with α = 109.5°.

model system we chose $[ReO_2H_2]^n$ (**3**), where the hydrides model the alkyl ligands. This substitution has been used in other studies with good results.[19]

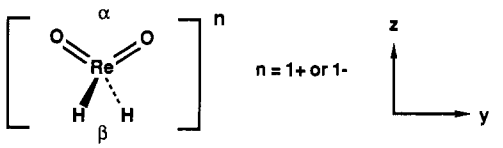

3

The first step in our analysis was to establish whether the model system and theoretical method would reproduce the distortion.[20] We also wanted to determine if the d^0 "core" has a great influence in setting the geometry.[21] In Figure 4a is shown total energy curves for variation of the angle O–Re–O, α, with fixed angle H–Re–H, β = 109.5°, for the d^0 and d^2 models $[ReO_2H_2]^n$, n = 1+ and 1–, respectively. In Figure 4b is shown the analogous curves for variation of the angle β with fixed angle α = 109.5°. In both cases the energy is relative to an arbitrary zero of energy at α, β = 109.5°.

The relative total energy curves in Figure 4 reveal the following features:

(a) Variation of α in Figure 4a for the d^2 model shows a steep descent into a minimum for ~160°, an opened O–Re–O angle. The d^0 core model's energy is relatively flat in the range α = 100–140°.

(b) Variation of β in Figure 4b for the d^2 model gives a minimum for ~80°, a closed H–Re–H angle. A second minimum near β = 180° is also observed, but it is more than 1.2 eV above the aforementioned one. The total energy for the d^0 model is relatively flat in the range β = 90–150°.

With regard to the results in Figure 4, it should be noted that we have varied α and β by 10° (5° near the minima) in the range 60–180° and found a geometry with α = 160° and β = 87° to be the minimum energy structure for the d^2 model. A shallow higher energy minimum is also observed at α, $\beta \approx$ 170°, a nearly square planar geometry. The total energy surface for the d^0 case is very flat in the range α, β = 100–130° with no clear minimum.

From these results we conclude the following:

(a) The extended Hückel method and the model system reproduce the gross features of the experimentally observed distortion in $[ReO_2(CH_2CMe_3)_2]^-$.

(b) Electronic factors from the d^0 core do not strongly influence the geometry of the d^2 model, and therefore, the geometry of d^2 $[ReO_2H_2]^-$ is set by its highest occupied molecular orbital.

Concerning point b, the calculations also suggest that d^0 $[MO_2(alkyl)_2]$ complexes should have geometries that are dependent upon steric factors and, in particular, bulky alkyl ligands should produce large C–M–C angles.[22] Unfortunately, structural studies of d^0 $[MO_2(alkyl)_2]$ have not been reported, so a comparison with experimental results is not possible. (We have prepared $[MoO_2(CH_2CMe_3)_2]$ but have not been able to grow crystals suitable for an X-ray structure determination.) A less direct comparison may be made to the d^0 dioxo halides, since the structures of $[MoO_2Cl_2]$ and two chromyl halides are known from electron diffraction studies. The geometry of the molybdenum complex is reported to be close to tetrahedral, but the experimental error is too large for meaningful comparison.[23] The structures of $[CrO_2X_2]$, X = Cl and F, are more precisely known.[24] They

(18) Burdett, J. K. *Molecular Shapes*; Wiley: New York, 1980; pp 35–37.
(19) Tatsumi, K.; Hoffmann, R.; Yamamoto, A.; Stille, J. K. *Bull. Chem. Soc. Jpn.* **1981**, *54*, 1857. Goddard, R. J.; Hoffmann, R.; Jemmis, E. D. *J. Am. Chem. Soc.* **1980**, *102*, 7667.
(20) This work is predated by a theoretical study of the electron-rich ML_4 complexes: Summerville, R. H.; Hoffmann, R. *J. Am. Chem. Soc.* **1976**, *98*, 7240.
(21) A general theoretical study of d^0 cis dioxo complexes can be found in: Tatsumi, K.; Hoffmann, R. *Inorg. Chem.* **1980**, *19*, 2656.
(22) It should be noted that nearly all d^0 cis-dioxo complexes have O–M–O angles in the range 102–114°. These are primarily octahedral complexes. See ref 21 and references therein.
(23) Skinner, H. A. Thesis, Oxford University, 1941. Quoted in: Wells, A. F. *Structural Inorganic Chemistry*, 5th ed.; Oxford University Press: Oxford, England, 1984; p 483.

are reported to have C_{2v} structures with slightly closed O–Cr–O and opened X–Cr–X angles, but both angles are within 5° of 109°. We are not certain what the factors are that influence the distortions in the chromyl halides, but since the distortions are opposite to that observed in the d^2 anions, it is clear that the same factors cannot be a major driving force in setting the d^2 complex geometries.

Since the calculations adequately reproduce the distortion in the d^2 anion, we can use the details of the calculational results to rationalize the experimental geometry. In this regard, we have traced the evolution of the molecular orbitals of $[ReO_2H_2]^-$ in Walsh diagrams (Figure 5). We will discuss the results of the analysis in the context of **4**, where we give the calculated level

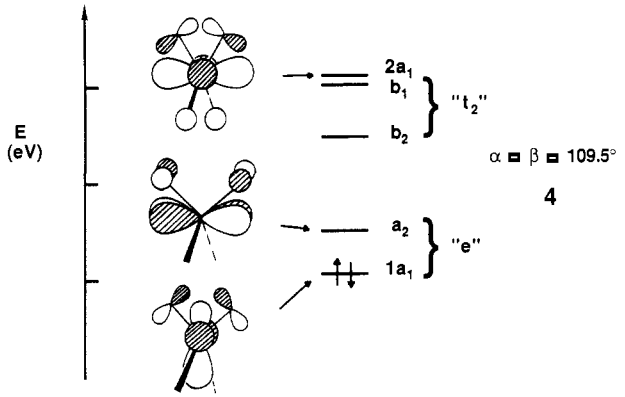

ordering of the d-block molecular orbitals and schematic drawings of the HOMO, LUMO, and one high-lying orbital, $2a_1$, for $[ReO_2H_2]^-$ with $\alpha, \beta = 109.5°$.

The gross level ordering in **4** of two below three is the expected crystal field splitting. In the coordinate system shown in **3** the lower energy "e" set of **4** is composed of one mainly xy orbital, a_2, and another mainly z^2 orbital, $1a_1$. The $1a_1$ HOMO also has metal p_z (7%) and $x^2 - y^2$ (13%) character. Both the a_1 HOMO and a_2 LUMO are Re–O π antibonding and have approximately 10% and 20% oxygen orbital character, respectively. There is no hydride contribution to the a_2 orbital since the H's lie in a node. For the HOMO the H's lie in a node with respect to the z^2 contribution (at $\alpha, \beta = 109.5°$) but can interact with the p_z and $x^2 - y^2$ orbitals and this generates 2% hydride character in the MO. The higher energy "t_2" set in **4** consists of mainly yz (b_2), xz (b_1), and $x^2 - y^2$ ($2a_1$).

The Walsh diagrams for angular variation from the tetrahedral geometry show the following features. As α is made larger (Figure 5a), the $1a_1$ HOMO is stabilized and the a_2 LUMO is destabilized. The HOMO is stabilized because π antibonding between the Re and the oxo ligands within the MO is reduced (**4**). The LUMO is destabilized because the motion increases the π antibonding between the Re and oxo ligands.

When the angle β is made smaller (Figure 5b), there can be no effect on the a_2 LUMO, but the $1a_1$ HOMO is stabilized by the distortion. This is in spite of the fact that the motion does not greatly affect the Re–H bonding. We have traced the HOMO stabilization in this case to a second-order perturbation mixing involving the high-energy MO $2a_1$ that is primarily $x^2 - y^2$ in character. It mixes into $1a_1$ with a positive sign for the phasing shown in **4**, and this reduces Re–O π antibonding in the HOMO.

The level crossings at the right in Figure 5b involving the orbitals $1a_1$, a_2, and b_1 account for the discontinuity and the second higher energy minimum in the total energy curve shown in Figure 4b. The level crossing is a consequence of the stabilization of b_1, an orbital primarily xz in character. The MO b_1 is Re–H σ antibonding at the tetrahedral geometry, and this is reduced to a nearly nonbonding interaction at $\beta = 180°$. While it is tempting to speculate that the level ordering at the opened angle (b_1 HOMO) applies to the case of the flattened-tetrahedral complex $[W(O\text{-}2,6\text{-}i\text{-}Pr_2Ph)_4]$ ($\alpha, \beta \approx 168°$),[3d] it is probably not correct. The level ordering for the tungsten complex will not be the same as that shown at the right in Figure 5b because of π antibonding from the alkoxides that will push a_2 and b_1 above $1a_1$ in energy.[25]

In summary, the calculations reveal that the geometry of the model for $[ReO_2(CH_2CMe_3)_2]^-$ is controlled by the HOMO and that the effect of distorting the geometry from tetrahedral is the stabilization of the HOMO by reduction of π antibonding between the Re and the oxo ligands. The distortion also serves to widen the HOMO–LUMO gap (1.1 eV at the experimental geometry of the anion in $[NEt_4][ReO_2(CH_2CMe_3)_2]$), and this accounts nicely for the observed diamagnetism in **2a–c**.

Concluding Remarks. We have shown that chemical reduction of the d^1–d^1 complex $[Re_2(\mu\text{-}O)_2O_2(CH_2CMe_3)_4]$ gives diamagnetic d^2 $[ReO_2(CH_2CMe_3)_2]^-$ in high yield when the reducing agents are Li/Hg and Na/Hg. Structural studies for the Li^+ and $[NEt_4]^+$ salts show that the d^2 anions are significantly distorted from a tetrahedral geometry. Calculations show that the distortion reduces π antibonding between the Re and the oxo ligands in the HOMO.

Among the known d^2 four-coordinate complexes the distortion observed in the anion $[ReO_2(CH_2CMe_3)_2]^-$ is unique,[26] but the complex $[W(O\text{-}2,6\text{-}i\text{-}Pr_2Ph)_4]$ is partially related to $[ReO_2(CH_2CMe_3)_2]^-$.[3d] The W complex has a severely flattened structure with opened RO–W–OR angles (~168°) analogous to the opened O–Re–O angle in $[ReO_2(CH_2CMe_3)_2]^-$. The phenoxide ligands of the W complex and the oxide ligands of the Re complex are electronically related as well in that both $p\pi$ orbitals of the phenoxides participate in π bonding to the metal through the agency of opened W–O–C angles (154–159°). Of course, the difference between the two complexes is the closed angle between the alkyl ligands in the anion. As our calculations show, π-bonding effects dominate and the angle between the alkyl ligands, which have no π-bonding capability, is set by the π bonding between the rhenium and oxo ligands.

We are now examining the chemistry of the anions, especially their reactivity with electrophiles and their use as "ligands" in transition-metal and main-group complexes. We also wish to prepare and structurally characterize analogous anions with different ligand sets (e.g. S or O, alkoxides or thiolates for alkyls) in order to examine the effect the perturbation will have on the structures.

Acknowledgment. This work was supported by the donors of the Petroleum Research Fund, administered by the American Chemical Society, and by a grant from the Research Corp. D.M.H. is a 1986–1987 Du Pont Young Faculty Fellow.

Registry No. **1**, 110091-18-4; **1**-^{18}O, 110391-52-1; **2a** (M = Li), 110391-54-3; **2a** (M = $Li(CH_3CN)_2$), 110391-56-5; **2b**, 110391-57-6; **2c**, 110391-58-7; **2c**-^{18}O, 110391-60-1; 3^+, 110391-61-2; 3^-, 110391-62-3; $ReO_3(OSiMe_3)$, 16687-12-0; $Al(CH_2CMe_3)_3(THF)$, 110391-53-2; $Zn(CH_2CMe_3)_2$, 54773-23-8; $^{18}OH_2$, 14314-42-2.

Supplementary Material Available: Complete tables of fractional coordinates and thermal parameters, a complete listing of bond distances and angles, and a ball and stick plot of $[Re_2(\mu\text{-}O)_2O_2(CH_2CMe_3)_4]$, complete tables of fractional coordinates and thermal parameters for $\{[Li(CH_3CN)_2][ReO_2(CH_2CMe_3)_2]\}_2$ and $[NEt_4][ReO_2(CH_2CMe_3)_2]$, and a packing diagram for $[NEt_4][ReO_2(CH_2CMe_3)_2]$ (10 pages); listings of F_o and F_c for all three complexes (18 pages). Ordering information is given on any current masthead page.

(24) Garner, C. D.; Mather. R.; Dove, M. F. A. *J. Chem. Soc., Chem. Commun.* **1973**, 633. Palmer, K. J. *J. Am. Chem. Soc.* **1938**, *60*, 2360. French, R. J.; Hedberg, L.; Hedberg, K.; Gard, G. L.; Johnson, B. M. *Inorg. Chem.* **1983**, *22*, 892. Marsden, C. J.; Hedberg, L.; Hedberg, K. *Inorg. Chem.* **1982**, *21*, 1115.

(25) In ref 20 D_{2d} distortions for MH_4 are discussed in detail.

(26) While this paper was being revised, the structure of $[OsO_2(mesityl)_2]$ was published. It is also distorted with O–Os–O = 136° and C–Os–C = 96.0°. Stravropoulos, P.; Edwards, P. G.; Behling, T.; Wilkinson, G.; Motevalli, M.; Hursthouse, M. B. *J. Chem. Soc., Dalton Trans.* **1987**, 169.